

Title	Loading effect in copper(II) oxide cluster-surface-modified titanium(IV) oxide on visible- and UV-light activities
Author(s)	Jin, Qiliang; Fujishima, Musashi; Iwaszuk, Anna; Nolan, Michael; Tada, Hiroaki
Publication date	2013-10-16
Original citation	Jin, Q., Fujishima, M., Iwaszuk, A., Nolan, M. and Tada, H (2013) 'Loading effect in copper(II) oxide cluster-surface-modified titanium(IV) oxide on visible- and UV-light activities', Journal of Physical Chemistry C, 117(45), pp. 23848-23857. http://pubs.acs.org/doi/abs/10.1021/jp4085525
Type of publication	Article (peer-reviewed)
Link to publisher's version	http://dx.doi.org/10.1021/jp4085525 Access to the full text of the published version may require a subscription.
Rights	This document is the Accepted Manuscript version of a Published Work that appeared in final form in Journal of Physical Chemistry C, copyright © American Chemical Society after peer review and technical editing by the publisher. To access the final edited and published work see http://pubs.acs.org/doi/abs/10.1021/jp4085525
Item downloaded from	http://hdl.handle.net/10468/2925

Downloaded on 2017-02-12T11:52:56Z

Loading Effect in Copper(II) Oxide Cluster-Surface Modified Titanium(IV) Oxide on the Visible- and UV-Light Activities

Qiliang Jin,^a Musashi Fujishima,^a Michael Nolan,^{b*} Hiroaki Tada^{a*}

^a Department of Applied Chemistry, School of Science and Engineering, Kinki University, 3-4-1, Kowakae, Higashi-Osaka, Osaka 577-8502, Japan. ^b Tyndall National Institute, University College Cork, Lee Maltings, Prospect Row, Cork, Ireland.

Supporting Information Placeholder

ABSTRACT: Cu(acac)₂ is chemisorbed on TiO₂ particles [P-25 (anatase/rutile = 4/1 w/w), Degussa] via coordination by surface Ti-OH groups without elimination of the acac-ligand. Post-heating of the Cu(acac)₂-adsorbed TiO₂ at 773 K yields molecular scale copper(II) oxide clusters on the surface (CuO/TiO₂). The copper loading amount (Γ Cu-ions nm⁻²) is controlled in a wide range by the Cu(acac)₂ concentration and the chemisorption-calcination cycle number. Valence band (VB)-X-ray photoelectron and photoluminescence spectroscopy indicated that the VB maximum of TiO₂ rises up with increasing Γ , while vacant mid-gap levels are generated. The surface modification gives rise to visible-light activity and concomitant significant increase in UV-light activity for the degradation of 2-naphthol and p-cresol. Prolonging irradiation time leads to the decomposition to CO₂, of which amount increases in proportion to irradiation time. The photocatalytic activity strongly depends on the loading, Γ , with an optimum value of Γ for the photocatalytic activity. Electrochemical measurements suggest that the surface CuO clusters promote the reduction of adsorbed O₂. First principles density functional theory (DFT) simulations clearly show that at $\Gamma < 1$, unoccupied Cu 3d levels are generated in the mid-gap region, and at $\Gamma > 1$, the VB maximum rises and the unoccupied Cu 3d levels move to the conduction band minimum of TiO₂. These results suggest that visible-light excitation of CuO/TiO₂ causes the bulk-to-surface interfacial electron transfer at low coverage and the surface-to-bulk interfacial electron transfer at high coverage. We conclude that the surface CuO clusters enhance the separation of photogenerated charge carriers by the interfacial electron transfer and the subsequent reduction of adsorbed O₂ to achieve the compatibility of high levels of visible and UV-light activities.

1. INTRODUCTION

Much effort has been devoted to the visible-light activation of TiO₂ for the applications as the environmental catalyts and self-cleaning materials.^{1,2} A conventional approach for the material modification is substitutional cation or anion doping at titanium or oxygen sites.³⁻¹⁰ Since there are many issues with doping, including solubility, stability and charge recombination, there is need to find alternative ways to shift the band gap of TiO₂ in order to make it more efficient in terms of visible-light absorption. Recently, visible-light activation of TiO₂ has been achieved by metal halide- and metal ion-grafting¹¹⁻¹⁶ and the surface modification with metal oxide clusters.¹⁷⁻²⁴ Among them, Cu²⁺ ion and CuO have attracted much interest as a promising surface modifier.²⁵⁻³² Interestingly, Irie et al. have shown that Cu²⁺-grafted TiO₂ (Cu²⁺/TiO₂) prepared by the impregnation method has oxidation ability sufficient for completely decomposing 2-propanol under visible-light irradiation.²⁸ Even if visible-light activity appears, it is usually much smaller than UV-light activity, and thus, the compatibility of high visible and UV-light activities is important from a viewpoint of effective sunlight use. However, UV-light activity has not been reported for the Cu²⁺/TiO₂ system and CuO-surface modified TiO₂. We have recently reported that FeO_x and NiO cluster-surface modified TiO₂ prepared by the chemisorption-calcination cycle (CCC) technique shows high photocatalytic activities under illumination of visible- and UV-light.¹⁷⁻²¹ In both the systems, strong dependence of the photocatalytic activity on the loading amount of the clusters is observed,¹⁷⁻²¹ but the reason has not been fully understood.

Herein we show that the surface modification of TiO₂ (P-25, Degussa) with molecular scale copper(II) oxide clusters by the CCC technique (CuO/P-25) causes visible-light activity and a

significant increase in the UV-light activity. P-25 (anatase/rutile = 4/1 w/w, specific surface area = 50 m² g⁻¹) is known to have the highest level of UV-light activity among the commercial TiO₂, and is widely used as a high standard photocatalyst. The strong dependence of the photocatalytic activity on the loading amount of CuO clusters is discussed at an electronic level on the basis of the results from spectroscopic experiments and first principles density functional theory (DFT) simulations.

2. EXPERIMENTAL SECTION

2.1 Catalyst preparation. TiO₂ particles (anatase/rutile = 4/1 w/w, specific surface area = 50 m² g⁻¹, P-25, Degussa) were used as a standard photocatalyst. After TiO₂ particles (2 g) had been added to 200 mL of a Cu(acac)₂ acetonitrile solution, they were allowed to stand for 24 h at 298 K. The Cu(acac)₂ concentration was changed from 0.1 mM to 7.0 mM. The solid samples were separated by centrifugation and washed twice with the solvent for the physisorbed complexes to be removed. Then, they were dried in vacuum at room temperature, followed by heating in air at 773 K for 1 h. For electrochemical measurements, mesoporous TiO₂ nanocrystalline film electrodes were used. A paste containing anatase TiO₂ particles with a mean size of 20 nm (PST-18NR, Nikki Syokubai Kasei) was coated on F:SnO₂-film coated glass substrates (12 Ω/□) by a squeegee method, and the sample was heated in air at 773 K to form mesoporous-TiO₂ films (mp-TiO₂/FTO).

2.2 Catalyst characterization. The Cu loading amount was determined by inductively coupled plasma spectroscopy (ICPS-7510, Shimadzu). The sample (0.1 g) was dispersed to hot conc. H₂SO₄ (5 mL), and the deposits were thoroughly

dissolved into the solution by stirring. The solution was diluted 5 times in volume with water, and then the Cu concentration was measured. UV-vis diffuse reflectance spectrum of CuO/TiO₂ was recorded on a Hitachi U-4000 spectrophotometer. Transmission electron microscopic (TEM) observation and energy dispersive X-ray (ED) spectroscopic measurements were performed using a JEOL JEM-3000F and Gatan Imaging Filter at an applied voltage of 300kV. X-ray photoelectron spectroscopic (XPS) measurements were performed using a Kratos Axis Nova X-ray photoelectron spectrometer with a monochromated Al K α X-ray source ($h\nu = 1486.6$ eV) operated at 15 kV and 10 mA. The take-off angle was 90°, and multiplex spectra were obtained for Cu2p photopeaks. All the binding energies (E_B) were referenced with respect to the C1s at 284.6 eV. The electrochemical properties of the CuO/mp-TiO₂/FTO electrodes were measured in 0.1 M NaClO₄ aqueous solution in a regular three-electrode electrochemical cell using a galvanostat/potentiostat (HZ-5000, Hokuto Denko). Glassy carbon and an Ag/AgCl electrode (TOA-DKK) were used as a counter electrode and a reference electrode, respectively.

2.3 Photocatalytic activity evaluation. 50 mL of 1.0×10^{-5} M 2-naphthol solution (solvent, acetonitrile : water = 1 : 99 v/v) or 5.0×10^{-4} M p-cresol solution (solvent, water) was placed in a double-jacket type reaction cell made of borosilicate glass, and then P-25 (Degussa) or CuO/P-25 particles (0.1 g) was added. The reaction cell was irradiated with a Xe lamp (Wacom XRD-501SW) through a band-pass filter (33U, SIGMA KOKI CO., Ltd.) superposed on FTO-coated glass (two pieces of FTO glass for 2-naphthol and a piece of FTO glass for p-cresol) transmitting only the 330-400 nm range for the UV-light photocatalytic activity evaluation and a high pass filter (L-42, Toshiba) to cut off UV-light for the visible-light-induced activity test. The irradiation conditions are as follows: for 2-naphthol UV-light ($330 < \lambda < 400$ nm, $I_{320-400 \text{ nm}} = 0.5 \text{ mW cm}^{-2}$) and visible-light ($\lambda > 400$ nm, $I_{420-485 \text{ nm}} = 1.0 \text{ mW cm}^{-2}$); for p-cresol UV-light ($330 < \lambda < 400$ nm, $I_{320-400 \text{ nm}} = 2 \text{ mW cm}^{-2}$) and visible-light ($\lambda > 400$ nm, $I_{420-485 \text{ nm}} = 2 \text{ mW cm}^{-2}$). Three mL of the solution was sampled every 15 min, and the absorbance at $\lambda = 224$ nm was measured using a spectrometer (UV-1800, Shimadzu) to determine the concentration of 2-naphthol. The p-cresol concentration was determined by high performance liquid chromatography [SPD-6A, Shimadzu; column = Fluofix INW425 4.6×250 mm (NEOS), mobile phase water-ethanol (3/7 v/v), $\lambda = 277$ nm].

2.4 CuO-TiO₂ Calculations. CuO-modified TiO₂ rutile (110) and anatase (001) surfaces are modelled using a three dimensional periodic slab model with the VASP code.³³ The cut-off for the kinetic energy is 396 eV. The valence electrons are described by a plane wave basis set and include 4 valence electrons for Ti, 6 for O and 11 for Cu. The exchange-correlation functional is the generalised gradient approximation of Perdew-Wang (PW91).^{34,35} We used the Monkhorst-Pack scheme for k-point sampling with a (2 \times 2 \times 1) sampling grid. The model anatase (001) surface is unreconstructed and is terminated by two-fold coordinated oxygen atoms while the Ti atoms in the surface layer are 5-fold coordinated. The (110) rutile surface is terminated by two-fold coordinated bridging oxygen atoms and the next sublayer consists 6-fold and 5-fold coordinated Ti atoms. We

employed a (2 \times 4) surface supercell for each TiO₂ surface and a larger (4 \times 4) surface supercell for some calculations, in order to reduce periodic interactions between adsorbed CuO nanoclusters. The free CuO nanoclusters are calculated in the same supercell as the corresponding CuO-modified TiO₂ and the same technical parameters are used. The clusters were deposited on both TiO₂ surfaces and fully relaxed. The adsorption energy was computed from:

$$E_{\text{ads}} = E((\text{CuO})_n\text{-TiO}_2) - \{E((\text{CuO})_n) + E(\text{TiO}_2)\} \quad (1)$$

Where $E((\text{CuO})_n\text{-TiO}_2)$ is the total energy of the (CuO)_n nanocluster, with n CuO units, supported on the TiO₂ surface. $E((\text{CuO})_n)$ and $E(\text{TiO}_2)$ are the total energies of the free (CuO)_n cluster and the bare TiO₂ surface respectively. A negative adsorption energy signifies that the cluster adsorption is more stable than a separated cluster and surface.

The calculations were carried out using DFT corrected for on-site Coulomb interactions, DFT+ U ,³⁶⁻⁴⁰ where we applied $U = 4.5$ eV on the Ti 3d states⁴¹ and for Cu in CuO (with Cu²⁺ states), we apply $U = 4$ eV, a typical value from the literature.⁴² The + U correction results in a relatively good description of the d states in oxidised and reduced Ti and in CuO.

3. RESULTS AND DISCUSSION

The adsorption isotherm of Cu(acac)₂ on P-25 from acetonitrile solution was measured at 298 K. As shown in Figure 1A, the adsorption apparently obeys the Langmuir behavior. From the Langmuir plot (inset in Figure 1A), the saturated adsorption amount and the adsorption equilibrium constant were calculated to be 0.54 ions nm⁻² and $1.34 \times 10^3 \text{ M}^{-1}$, respectively. These results suggest that Cu(acac)₂ is chemisorbed on P-25. In the present system, the copper loading amount was expressed by the number of copper ions per unit surface area of

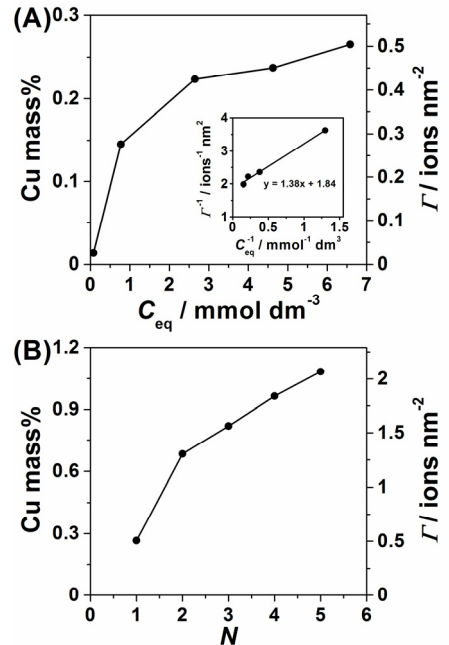


Figure 1. (A) Adsorption isotherm of Cu(acac)₂ on P-25 from acetonitrile solution measured at 298 K. The inset shows the Langmuir plot: the x-axis denotes the amount of Cu adsorbed per unit mass of TiO₂. (B) Plots of Γ vs. chemisorption-calcination cycle number (N) ($[\text{Cu}(\text{acac})_2]_0 = 7 \text{ mM}$).

TiO₂ (Γ ions nm⁻²). Figure 1B shows plots of Γ vs. CC cycle number (N) at the initial Cu(acac)₂ concentration = 7 mM. The Γ increases with an increase in N . In the CCC technique, the Cu loading amount can be precisely controlled by the Cu(acac)₂ concentration at $\Gamma < 0.5$ and by N at $\Gamma > 0.5$.

To further study the mechanism of Cu(acac)₂ adsorption on

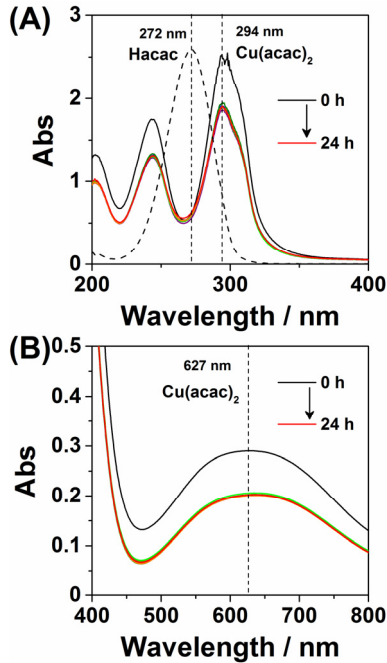


Figure 2. (A) UV (A) and visible (B) absorption spectral change of a Cu(acac)₂ solution with adsorption.

P-25, the absorption spectral change of the solution was traced with adsorption. In the UV range (Figure 2A), Cu(acac)₂ and free acetylacetonate (Hacac) have absorption bands at 294 and 272 nm due to the $\pi-\pi^*$ transition, respectively. As the adsorption proceeds, the absorption at 294 nm weakens, but the absorbance at 272 nm is invariant. In the visible range (Figure 2B), there is a weak d-d transition absorption of Cu(acac)₂ around 625 nm. The absorption intensity also decreases with adsorption. This finding indicates that Cu(acac)₂ is adsorbed on P-25 without liberation of the acac-ligand.

To gain information about the states of the adsorbed species before and after heating, diffuse Fourier-transformed infrared spectra (DRIFT) were measured. Figure 3 shows difference DRIFT spectra for Cu(acac)₂/TiO₂ minus TiO₂ (a) and

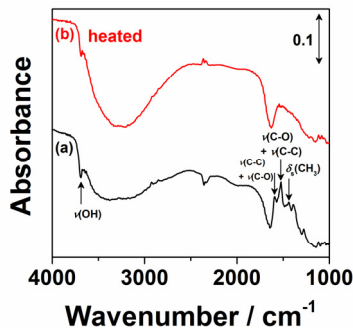


Figure 3. Difference DRIFT spectra: Cu(acac)₂/TiO₂ minus TiO₂ (a) and Cu(acac)₂/TiO₂ heated at 773 K minus TiO₂ (b).

Cu(acac)₂/TiO₂ heated at 773 K minus TiO₂ (red). In spectrum (a), three absorption peaks are present at 1593, 1527, and 1374 cm⁻¹, which can be assigned to the combination of $\nu(\text{C-C}) + \nu(\text{C-O})$, the combination of $\nu(\text{C-O}) + \nu(\text{C-C})$, $\delta_s(\text{CH}_3)$, respectively.⁴³ Also, a negative signal due to the surface OH groups of P-25 (Ti₅-OH) appears at 3668 cm⁻¹.⁴⁴ These results above suggest that Cu(acac)₂ is chemisorbed on P-25 via the chemisorption via surface Ti-OH coordination without elimination of the acac-ligands. This is contrast to the Fe(acac)₃ adsorption on TiO₂, which proceeds via the ligand-exchange between the acetylacetonate ligand and the surface.¹⁸

To examine the oxidation state of the copper on the TiO₂ surface, UV-visible absorption spectra of the samples were measured. Cu²⁺/TiO₂ prepared by the impregnation method has an absorption tail in the 400-500 nm region in addition to the appreciable d-d transition absorption of Cu²⁺ ions at 700-800 nm, whereas the absorption edge is invariant.^{28,32} The former weak absorption was assigned to the transition from the VB(TiO₂) to vacant Cu²⁺ ion levels. Figure 4 shows UV-visible absorption spectra of the samples prepared by the CCC technique. In contrast to the spectra of Cu²⁺/TiO₂, band gap narrowing occurs with an absorption tail at 400-500 nm. At $\Gamma \geq 0.32$, the weak d-d transition band of Cu²⁺ ions appears at 700-800 nm. However, the absorption due to the interband transition of Cu₂O with a band gap of ~2 eV is absent.⁴⁵ These optical features indicate that unique copper oxide species with the oxidation state of +2 are formed by the CCC technique.

Also, X-ray photoelectron spectroscopic (XPS) measurements were performed. Figure 5 shows the Cu 2p-XP spectra for the copper oxide-surface modified P-25 with varying Γ . In the spectrum for the sample with $\Gamma = 0.015$, the signal due to the emission from the Cu2p3/2 orbital is observed at the binding energy (E_B) = 931.3 eV. Closer inspection is indicative of a slight shift in the E_B towards higher energy side with increasing Γ . In the spectrum for the sample with $\Gamma = 2.1$, the $E_B(\text{Cu}2p3/2)$ are located at 932.7 eV in addition to a shake-up satellite around 943.1 eV. These E_B values are significantly

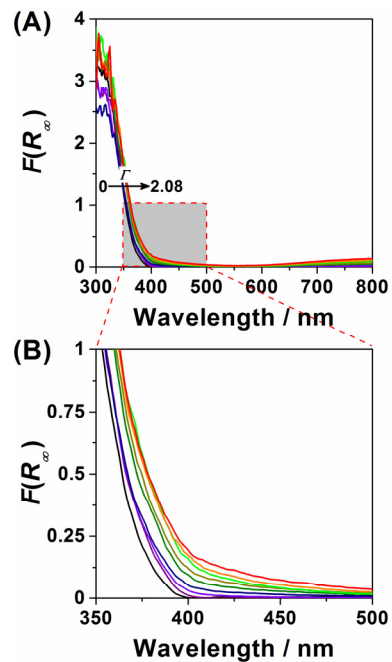


Figure 4. UV-visible absorption spectra of the samples prepared by the CCC technique: $F(R_\infty)$ denotes the Kubelka-Munk function.

lower than that for bulk CuO (933.8 eV).⁴⁶ It is known that the $E_B(\text{Cu}2p_{3/2})$ value shifts to lower binding energy as the loading amount of highly dispersed copper species decreases.⁴⁷ The $E_B(\text{Cu}2p_{3/2})$ value and the presence of the satellite peak indicate that the copper oxidation state is +2. Evidently, Cu(II) oxide clusters are formed on the TiO_2 surface in a highly dispersion state by the CCC technique. The copper(II) oxide species are formally shown as CuO below.

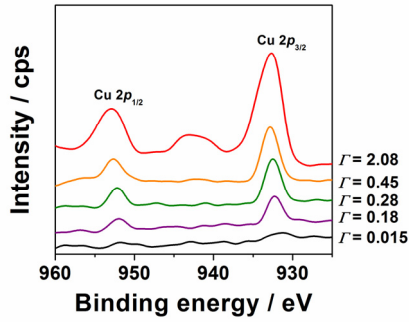
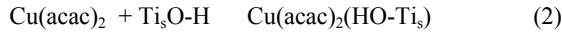


Figure 5. Cu 2p-XPS spectra for the copper oxide-surface modified P-25 with varying CuO loading (Γ).

On the basis of these results above, the mechanism of the CuO clusters on TiO_2 by the CCC technique can be written as follows:



Δ



Δ

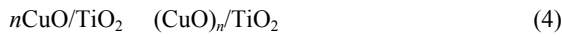


Figure 6 shows transmission electron micrographs (TEMs) of the samples with $\Gamma < 2.1$. No deposits are observed on the P-25 surface, whereas CuO particles with a mean size of ~ 5 nm are deposited on TiO_2 by the impregnation method.⁴⁸ In this manner, extremely small copper oxide clusters are formed on P-25 by the CCC technique. This would result from the strong chemisorption of $\text{Cu}(\text{acac})_2$ on P-25 (eq 2) to restrict the growth of the CuO clusters during the post-heating process (eq 4).

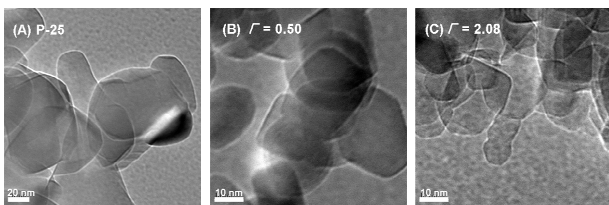


Figure 6. TEMs of the samples with varying Γ prepared by the CCC technique: (A) $\Gamma=0$, (B) $\Gamma=0.50$, (C) $\Gamma=2.08$.

2-Naphthol and p-cresol are widely used as a starting material of azo-dyes and a disinfectant, respectively. For evaluation of the photocatalytic activity of CuO/P-25, 2-naphthol and p-cresol with no absorption at $\lambda > 330$ nm were employed as model water pollutants. Both the degradations of 2-naphthol and p-cresol apparently followed the first-order rate law under irradiation of UV-light ($330 < \lambda < 400$ nm, $I_{320-400 \text{ nm}} = 0.5 \text{ mW cm}^{-2}$) and visible-light ($\lambda > 400$ nm, $I_{420-485 \text{ nm}} = 1.0 \text{ mW cm}^{-2}$).

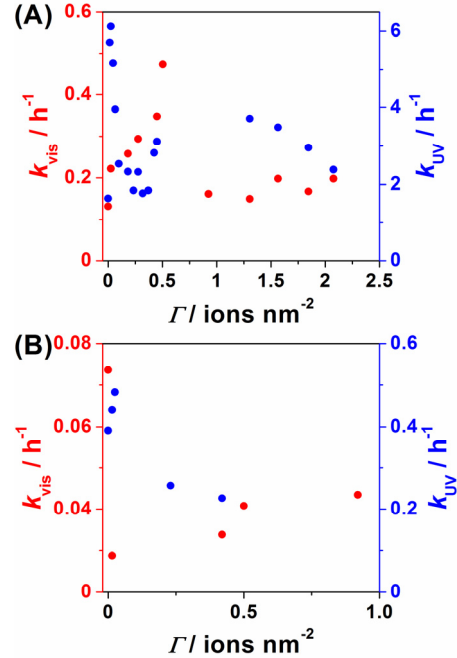


Figure 7. Plots of the rate constants for the degradations of 2-naphthol (A) and p-cresol (B) under irradiation of visible-light and UV-light as a function of CuO loading (Γ).

The activity was assessed by the pseudo-first-order rate constant (k/h^{-1}). Without photocatalysts or irradiation, the degradations of 2-naphthol and p-cresol hardly occurred. Figure 7A shows the rate constants for the 2-naphthol degradation under visible-light ($k_{\text{vis}}/\text{h}^{-1}$) and UV-light ($k_{\text{UV}}/\text{h}^{-1}$) as a function of Γ . Significant increases in both the visible- and UV-light activities are induced by the CuO surface modification. The k_{vis} value possesses a maximum of 0.47 h^{-1} at $\Gamma \approx 0.5$. Also, the k_{UV} abruptly increases to 6.1 h^{-1} at $\Gamma \approx 0.025$, which is greater than that for pristine P-25 by a factor of 3.4. While several unidentified intermediates were detected by HPLC, prolonging irradiation time resulted in the complete oxidation of 2-naphthol CO_2 . CuO/P-25 appears pale green before the reactions to change red, which suggesting the Cu^{2+} ions in the cluster are partially reduced to Cu^+ ions during the reaction.

On the other hand, Figure 7B shows the k_{vis} and k_{UV} values for the p-cresol degradation as a function of Γ . Both the plots exhibit profiles similar to those of the k vs. Γ plots for the 2-naphthol degradation, although the enhancing effect by the surface modification is smaller than that for the 2-naphthol degradation.

Valence band (VB)-XPS measurements were carried out to examine changes in the filled energy levels of CuO/P-25 with CuO loading. Figure 8A shows the VB-XP spectra for CuO/P-25 with varying Γ . The emission from the VB of TiO_2 primar-

ily consisting of occupied O2p orbitals extends from 2 to 9 eV. As shown in Figure 8B, the VB edge shifts upwards by ~ 0.7 eV with increasing Γ . The energy of the VB maximum is important because it determines the oxidation ability of the holes – a deep VB edge usually results in good oxidative ability and increasing the energy of the VB reduces the oxidative power of the holes. The effective mixing between the surface CuO cluster levels and the O2p states from the surface, as a result of the Ti-O-Cu interfacial bond is considered to yield a surface d sub-band dispersing around the energy level to overlap with the TiO₂ VB (see DFT simulation). These considerations explain the shift in the VB edge and the band gap narrowing of TiO₂ with CuO modification, i.e., the visible-light absorption of CuO/TiO₂ can mainly be attributed to the interfacial electron transfer from the d-subband to the conduction band (CB) of TiO₂. From the band gap for CuO ($\Gamma \approx 1.9$)/P-25 (~ 1.7 eV), the top of the surface d band is estimated to be situated at +1.8 V vs. standard hydrogen electrode (SHE) at pH 7. The electrode potentials are shown with respect to SHE below.

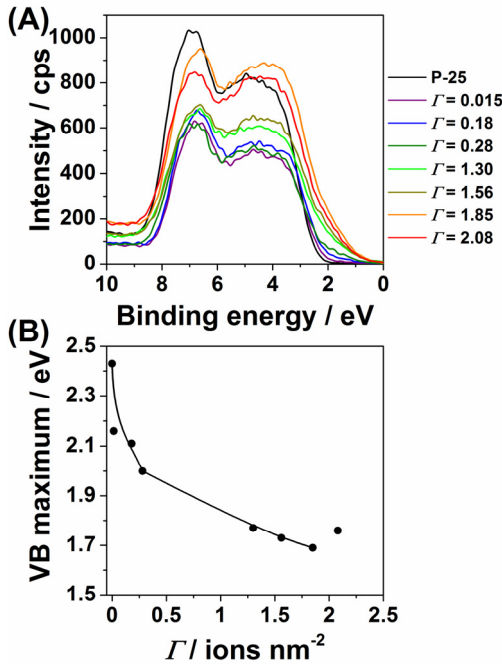


Figure 8. (A) VB-XP spectra for CuO/P-25. (B) Change in the position of the VB maximum level as a function of CuO loading (Γ).

Information about empty levels can be obtained by photoluminescence (PL) spectroscopy. Figure 9 shows PL spectra of CuO/P-25 with varying Γ at 77 K. P-25 has a broad emission band around 540 nm (E_1) in addition to the weak band-to-band emission at 400 nm (E_2). The E_1 signal intensity remarkably weakens with heating P-25 at 773 K for 1 h in air. This PL band was assignable to the emission from the surface oxygen vacancy levels of anatase TiO₂,⁴⁹ which are healed upon annealing. On modifying P-25 with CuO clusters, the PL intensity gradually decreases with an increase in Γ to disappear at $\Gamma = 2.1$. Concomitantly, a weak PL band (E_3) appears near 470 nm, which would arise from the emission from the CuO derived cluster levels. Consequently, the excited electrons in the CB of TiO₂ are preferentially transferred to the CuO cluster levels rather than the surface oxygen vacancy levels. As suggested by Irie et al., the visible-light-driven transition from the

VB of TiO₂ to the vacant CuO cluster levels is also possible (see DFT simulation).^{28,32}

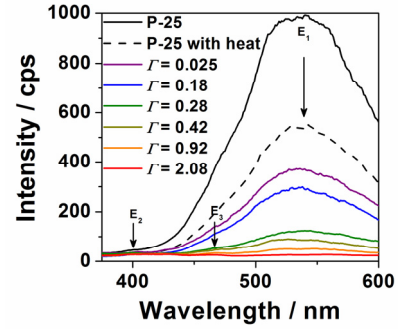


Figure 9. PL spectra of CuO/P-25 with varying CuO loading (Γ) at 77 K: excitation wavelength = 320 nm.

Further, the dark current (I)-potential (E) curves of the mp-TiO₂/FTO and CuO/mp-TiO₂/FTO electrodes were measured in the potential range between -0.4 and +0.4 V in 0.1 M NaClO₄ solutions. As shown in Figure 10, for the mp-TiO₂/FTO electrode, only small current flows in the potential range under deaerated conditions. Under aerated conditions, a current peak is observed at -0.3 V, which is close to the potential for one-electron reduction of O₂ ($E^0(\text{O}_2/\text{O}_2^-) = -0.28$ V).⁵⁰ On the other hand, for the CuO/mp-TiO₂/FTO electrode, a current peak due to the reduction of the surface Cu(II) oxides to the Cu(I) oxides appears at $\sim +0.05$ V. Interestingly, under aerated conditions, the reduction current significantly increases in the potential range from +0.25 to -0.2 V. Nosaka and co-workers have confirmed by means of electron spin resonance spectroscopy and chemiluminescence photometry that visible-light irradiation to Cu²⁺/TiO₂ yields Cu⁺ ions in vacuum and O₂⁻ ions in water.³² In the present system, there is a possibility that the interaction between the CuO species and O₂ molecule enhances the O₂ reduction, although multi-electron reduction of O₂ can not be excluded.²⁸ Thermodynamically, the multi-electron reduction is permitted ($E^0(\text{O}_2/\text{H}_2\text{O}_2) = +0.68$ V and $E^0(\text{O}_2/\text{H}_2\text{O}) = +1.23$ V), whereas one-electron reduction is impossible. Consequently, the surface Cu(II) oxide species on the TiO₂ surface would be reduced to Cu(I) oxide ones acting as a promoter for the O₂ reduction.

To understand the surface modification effect by CuO clusters (CuO)_{*n*} at an electronic level, we present the results from first principles DFT simulations. The cluster size n was changed to study the influence of the Cu-loading amount or Γ

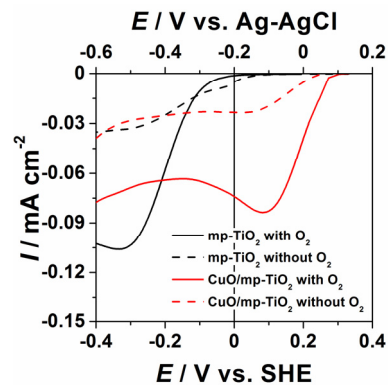


Figure 10. Dark current (I)-potential (E) curves of the mp-TiO₂/FTO and CuO/mp-TiO₂/FTO electrodes measured in 0.1 M NaClO₄ solutions.

on the electronic structure of TiO_2 . Figure 11 shows the atomic structure and projected electronic density of states (PEDOS), where the Cu and Ti 3d and O 2p EDOS are displayed, for rutile TiO_2 modified with $(\text{CuO})_n$ nanoclusters, with $n = 1 - 4$. Figure 12 shows the atomic structure and PEDOS for anatase modified with $(\text{CuO})_n$ nanoclusters. The Γ values of CuO, Cu_2O_2 and Cu_4O_4 nanoclusters on the rutile and anatase surfaces as are follows. On rutile: 0.64, 1.28 and 1.78 (on the (4×4) surface supercell) Cu atoms/ nm^2 and on anatase 0.85, 1.70 and 1.70 (on the (4×4) surface supercell) Cu atoms/ nm^2 .

For both anatase and rutile, the adsorption energies signify strong adsorption of the CuO nanoclusters at the respective surfaces, driven by formation of new interfacial Cu-O and Ti-O bonds between the cluster and surface and surface and cluster, respectively. For the same cluster size, the energy of adsorption on rutile is larger than that for anatase.

The surface modification by CuO clusters causes a significant change in the TiO_2 energy bands at the VB and conduction band (CB) edges, which are strongly dependent on n . For modification of rutile (110) with an isolated CuO cluster ($n = 1$) we find the appearance of unoccupied Cu 3d levels in the mid-gap region, while the top of VB rises albeit by a smaller amount. For anatase (001), modification with the CuO cluster also introduces the unoccupied Cu(II) state into the mid-gap region.

If we now consider the impact of the Cu-loading amount on rutile, we find interesting behavior in that, as the Γ increases, a significant rise in the top of VB is found, which is up to *ca.* 0.7 eV for Cu_4O_4 -modified rutile (110). At the same time, the unoccupied Cu(II) derived levels undergo an upwards energy shift, to approach the CB minimum of TiO_2 , e.g. for Cu_4O_4 -modified rutile (110), the unoccupied CuO states lie at the TiO_2 CB edge. This also results in a narrowing of the band gap compared to unmodified TiO_2 , but for a different reason to the smallest CuO nanocluster. In this case, it is the upwards shift in the VB edge with increased CuO loading that narrows the band gap.

In Figure 12, we show the atomic structure and PEDOS for anatase (001) modified with CuO nanoclusters. In this case,

while a similar trend in the nature of the electronic structure is observed in that the nature of the VB and CB edges depends on the loading amount of CuO clusters, we find a difference to modified rutile. For modified anatase, the unoccupied CuO states are rather deep in the energy gap, while the upwards shift of the VB edge is not as significant as seen for modified rutile.

Recently, Liu et al. has reported that loading Cu_2O particles smaller than 3 nm on TiO_2 nanosheets with $\{001\}$ facets shows a visible-light activity for degradation of phenol three times larger than that of N-doped TiO_2 .⁴⁶ In the nano-coupling system, the band energy of each component is essentially invariant, and the high visible-light activity can be explained in terms of the efficient charge separation resulting from the interfacial electron transfer from the CB(Cu_2O) to the CB(TiO_2). On the other hand, the molecular scale CuO clusters acts as an electronic modifier for TiO_2 . The action mechanism of the CuO clusters on the photocatalytic activity of P-25 is discussed in detail below. For isolated CuO cluster (or $n = 1$), visible-light irradiation can lead to the excitation of the electrons from the VB(TiO_2) to the unoccupied Cu 3d levels or the bulk-to-surface interfacial electron transfer as suggested by Irie et al.²⁸ Although Irie et al. do show a band gap reduction for their CuO clusters grafted by the impregnation method, that are larger than those prepared in the present work, they do not provide any analysis of the origin of the reduced band gap.

On the other hand, at $n \geq 2$, the DFT simulations and experimental results show clearly that excitation from the occupied surface CuO derived levels to the CB of TiO_2 or the surface-to-bulk electron transfer will likely dominate. Further evidence for this comes from the upwards shift in the VB edge with increasing Γ that tracks the decrease in the energy gap with CuO cluster loading. Similar shifts in the VB edge for other metal oxide-nanocluster modified TiO_2 are explained on the basis of the formation of new VB states coming from the oxide nanocluster.¹⁷⁻²¹ This interfacial electron transfer causes efficient charge carrier separation contributing to the increases in the photocatalytic activities and the reduction in the TiO_2

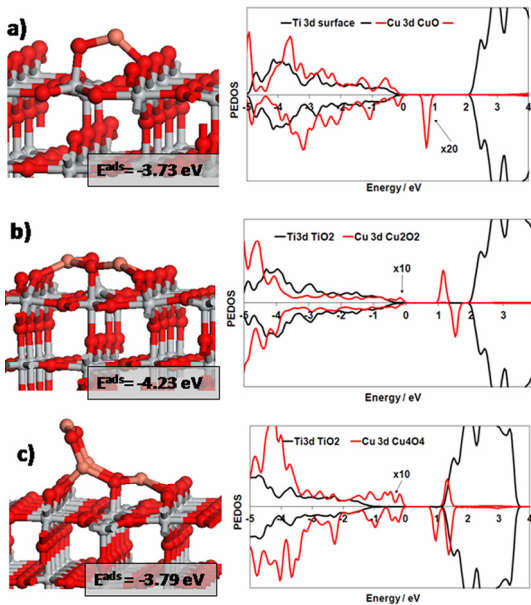


Figure 11. Atomic structure, adsorption energy in eV and Ti 3d and Cu 3d projected electronic density of states (PEDOS) for rutile TiO_2 modified with CuO, Cu_2O_2 and Cu_4O_4 clusters.

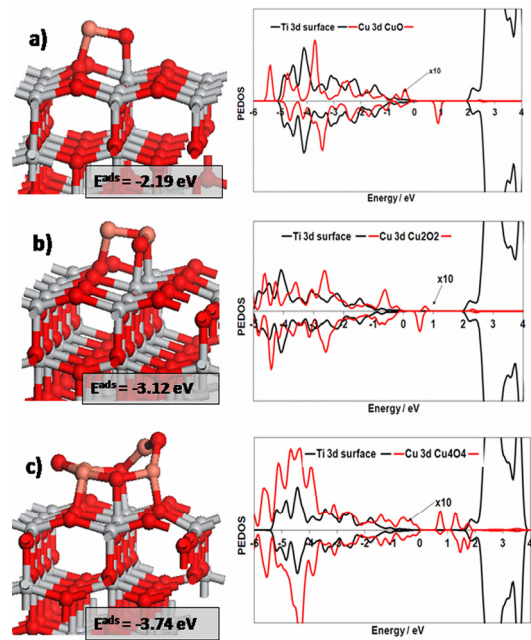


Figure 12. Atomic structure, adsorption energy in eV and Ti 3d and Cu 3d projected electronic density of states (PEDOS) for anatase TiO_2 modified with CuO, Cu_2O_2 and Cu_4O_4 clusters

derived PL signal.

In the cathodic process, the excited electrons in the CB of TiO₂ can be transferred to the surface CuO cluster levels, which enhances the electron transfer to O₂. Recently, we have shown that the TiO₂-photocatalyzed degradations of 2-naphthol and p-cresol proceed via the direct hole oxidation.⁵¹ In the anodic process, the holes in the VB of isolated CuO cluster-surface modified TiO₂ possess strong oxidation ability to decompose organic compounds including 2-naphthol and p-cresol. As the Γ increases, the visible-light absorption intensifies, whereas the rise in the VB maximum weakens the oxidation ability of the holes or the surface non-radiative recombination of the charge carriers may be enhanced. The balance between them would determine the optimum loading amount.

4. CONCLUSIONS

The CCC technique using Cu(acac)₂ as a precursor has formed molecular scale CuO clusters on the surfaces of TiO₂ particles (P-25, Degussa) in a highly dispersed state. Band gap narrowing occurs as a result of the surface modification with a very weak absorption due to the d-d transition. Also, visible-light activities for the degradations of 2-naphthol and p-cresol are induced concomitantly with the UV-light activities significantly increased. DFT simulation has indicated that the TiO₂ surface modification by a small amount of isolated CuO clusters yields unoccupied Cu 3d levels in the midgap region with the VB maximum hardly changed. However, as the loading amount increases, the experiments and simulations show that the VB maximum rises and furthermore the simulations show that the unoccupied Cu 3d levels approach the CB minimum, thus giving a different mechanism for band gap reduction. The enhanced visible-light absorption and increased charge separation efficiency lead to a remarkable increase in the photocatalytic efficiency with the CuO nanoclusters acting as a promoter for the reduction of O₂.

ASSOCIATED CONTENT

AUTHOR INFORMATION

Corresponding Author

h-tada@apch.kindai.ac.jp

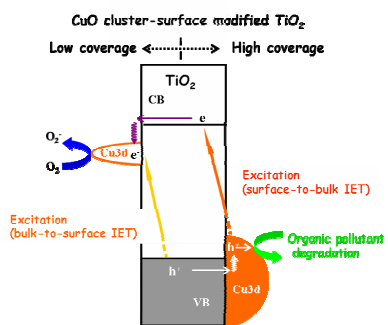
ACKNOWLEDGMENT

HT acknowledges supports from the Ministry of Education, Science, Sport, and Culture, Japan through a Grant-in-Aid for Scientific Research (C) No. 24550239, and Nippon Sheet Glass Foundation for Materials Science and Engineering, and by Sumitomo Foundation. MN and AI acknowledge support from Science Foundation Ireland (SFI) through the Starting Investigator Research Grant Program, project “EMOIN”, grant number SFI 09/SIRG/11620, and the European Commission through the COST Action CM1104 “Reducible Metal Oxides, Structure and Function”. We acknowledge access to computing resources at Tyndall provided by SFI and by the SFI and Higher Education Authority funded Irish Centre for High End Computing and the European Commission Partnership in Advanced Computing (PRACE, contracts RI-261557, RI-283493 and RI-312763) for access to the JUROPA Computer at Forschungszentrum Juelich through the DECI-9 initiative.

REFERENCES

- (1) Fujishima, A.; Zhang, X.; Tryk, D. A. *Surf. Sci. Rep.* **2008**, *63*, 515.
- (2) Hashimoto, K.; Irie, H.; Fujishima, A. *Jpn. J. Appl. Phys.* **2005**, *44*, 8269.
- (3) Asahi, R.; Morikawa, T.; Ohwaki, T.; Aoki, K.; Taga, Y. *Science* **2001**, *293*, 269.
- (4) Khan, S. U. M.; Al-Shahry, M. B.; Ingler Jr, W. B. *Science* **2002**, *297*, 2243.
- (5) Serpone, N. *J. Phys. Chem. B* **2006**, *110*, 24287.
- (6) Zhang, H.; Chen, G.; Bahnemann, D. W. *J. Mater. Chem.* **2009**, *19*, 5089.
- (7) Anpo, M.; Takeuchi, M. *J. Catal.* **2003**, *216*, 505.
- (8) Kitano, M.; Funatsu, K.; Matsuoka, M.; Ueshima, M.; Anpo, M. *J. Phys. Chem. B* **2006**, *110*, 25266.
- (9) Rajeshwar, K.; de Tacconi, N. R. *Chem. Soc. Rev.* **2009**, *38*, 1984.
- (10) Liu, G.; Wang, L.; Yang, H. G.; Cheng, H.-M.; Lu, G. Q. *J. Mater. Chem.* **2010**, *20*, 831.
- (11) Kisch, H. *Angew. Chem. Int. Ed.* **2012**, *51*, 2.
- (12) Kisch, H.; Zhang, L.; Lange, C.; Maier, W. F.; Antonius, C.; Meissner, D. *Angew. Chem. Int. Ed.* **1998**, *37*, 3034.
- (13) Murakami, N.; Chiyoya, T.; Tsubota, T.; Ohno, T. *Appl. Catal. A* **2008**, *348*, 148.
- (14) Irie, H.; Miura, S.; Kamiya, K.; Hashimoto, K. *Chem. Phys. Lett.* **2008**, *457*, 202.
- (15) Yu, H.; Irie, H.; Shimodaira, Y.; Hosogi, Y.; Kuroda, Y.; Miyachi, M.; Hashimoto, K. *J. Phys. Chem. C* **2010**, *114*, 16481.
- (16) Irie, H.; Shibamura, T.; Kamiya, K.; Miura, S.; Yokoyama, T.; Hashimoto, K. *Appl. Catal. B* **2010**, *96*, 142.
- (17) Tada, H.; Jin, Q.; Nishijima, H.; Yamamoto, H.; Fujishima, M.; Okuoka, S.-i.; Hattori, T.; Sumida, Y.; Kobayashi, H. *Angew. Chem. Int. Ed.* **2011**, *50*, 3501.
- (18) Jin, Q.; Fujishima, M.; Tada, H. *J. Phys. Chem. C* **2011**, *115*, 6478.
- (19) Nolan, M.; Iwaszuk, A.; Tada, H. *Aust. J. Chem.* **2012**, *65*, 624.
- (20) Jin, Q.; Ikeda, T.; Fujishima, M.; Tada, H. *Chem. Commun.* **2011**, *47*, 8814.
- (21) Iwaszuk, A.; Nolan, M.; Jin, Q.; Fujishima, M.; Tada, H. *J. Phys. Chem. C* **2013**, *117*, 2709.
- (22) Fujishima, M.; Jin, Q.; Yamamoto, H.; Tada, H.; Nolan, M. *Phys. Chem. Chem. Phys.* **2012**, *14*, 705.
- (23) Jin, Q.; Fujishima, M.; Nolan, M.; Iwaszuk, A.; Tada, H. *J. Phys. Chem. C* **2012**, *116*, 12621.
- (24) Jin, Q.; Arimoto, H.; Fujishima, M.; Tada, H. *Catalysts* **2013**, *3*, 444.
- (25) Ohno, T.; Murakami, N.; Tsubota, T.; Nishimura, H. *Appl. Catal. A* **2008**, *349*, 70.
- (26) Ohko, Y.; Noguchi, H.; Nakamura, Y.; Negishi, N.; Takeuchi, K. *J. Photochem. Photobiol. A* **2009**, *206*, 27.
- (27) Wu, Y.; Lu, G.; Li, S. *Catal. Lett.* **2009**, *113*, 97.
- (28) Irie, H.; Kamiya, K.; Shibamura, T.; Miura, S.; Tryk, D. A.; Yokoyama, T.; Hashimoto, K. *J. Phys. Chem. C* **2009**, *113*, 10761.
- (29) Lalitha, K.; Sadanandam, G.; Kumari, V. D.; Subrahmanyam, M.; Hebalkar, N. Y. *J. Phys. Chem. C* **2010**, *114*, 22181.
- (30) Yu, J.; Hai, Y.; Jaroniec, M. *J. Colloid Interface Sci.* **2011**, *357*, 223.
- (31) Kitano, S.; Hashimoto, K.; Kominami, H. *Appl. Catal. B : Environ.* **2011**, *101*, 206.
- (32) Nosaka, Y.; Takahashi, S.; Sakamoto, H.; Nosaka, A. *J. Phys. Chem. C* **2012**, *115*, 21283.
- (33) Kresse, G.; Hafner, J.; *Phys. Rev. B* **1994**, *49*, 1425.
- (34) Blöchl, P. E. *Phys. Rev. B* **1994**, *50*, 17953.

- (35) Perdew, J. P.; in *Electronic Structure of Solids '91*, eds. P. Ziesche, P. Eschrig, H. Akademie Verlag, Berlin, **1991**.
- (36) Morgan, B.J.; Watson, G.W. *Surf. Sci.* **2007**, *601*, 5034.
- (37) Anisimov, V. I.; Zaanen J.; Andersen, O. K. *Phys. Rev. B* **1991**, *44*, 943.
- (38) Dudarev, S. L.; Botton, G. A.; Savrasov, S. Y.; Humphreys C. J.; Sutton, A. P. *Phys. Rev. B* **1998**, *57*, 1505.
- (39) Ganduglia-Pirovano, M. V.; Hofmann, A.; Sauer, J. *Surf. Sci. Rep.* **2007**, *62*, 219.
- (40) Nolan, M.; Grigoleit, S.; Sayle, D. C.; Parker, S. C.; Watson, G. W. *Surf. Sci.* **2005**, *576*, 217.
- (41) Anisimov, W. J.; Zaanen, J.; Andersen, O. K. *Phys Rev B* **1991**, *44*, 3.
- (42) Wang, L.; Maxisch, T.; Ceder, G., *Phys. Rev. B*, **2006**, *73*, 195107.
- (43) Nakamoto, K. *Infrared and Raman Spectra of Inorganic and Coordination Compounds*, 4th ed.; Wiley-Interscience, New York, 1986.
- (44) Tada, H. *Langmuir* **1996**, *12*, 966.
- (45) Liu, L.; Gu, X.; Sun, C.; Li, H.; Deng, Y.; Gao, F.; Dong, L. *Nanoscale* **2012**, *4*, 6351.
- (46) Li, G.; Dimitrijevic, N. M.; Chen, L.; Rajh, T.; Gray, K. A. *J. Phys. Chem. C* **2008**, *112*, 19040.
- (47) Chary, K. V. R.; Sagar, G. V.; Srikanth, C. S.; Rao, V. V. *J. Phys. Chem. B* **2007**, *111*, 543.
- (48) Qiu, X.; Miyachi, M.; Sunada, K.; Minoshima, M.; Liu, M.; Lu, Y.; Li, D.; Sihmodaira, Y.; Hosogi, Y.; Kuroda, Y.; Hashimoto, K. *ACS Nano* **2012**, *6*, 1609.
- (49) Shi, J.; Chen, J.; Feng, Z.; Chen, T.; Lian, Y.; Wang, X.; Li, C. *J. Phys. Chem. C* **2007**, *111*, 693.
- (50) *Denki Kagaku Binran 5th Ed. (Handbook of Electrochemistry)*, Electrochem. Soc. Jpn. Ed., Maruzen, Tokyo, 2000.
- (51) Tada, H.; Jin, Q.; Kobayashi, H. *ChemPhysChem* **2012**, *13*, 3457.



Insert Table of Contents artwork here